Helium isotope disequilibrium and geochronology of glassy submarine basalts

David W. Graham, William J. Jenkins
Mark D. Kurz & Rodey Batiza*†

Department of Chemistry, Woods Hole Oceanographic Institution, Woods Hole, Massachusetts 02543, USA
* Department of Earth and Planetary Sciences, Washington University, St. Louis, Missouri 63130, USA

The (U+Th)/He dating method is the oldest method of geochronology that involves radioactivity, but historically it has not been particularly successful. Even when problems of poor helium retention and loss due to radiation damage are circumvented by analysing suitable mineral phases[1–4], problems frequently remain with inherited helium[5,6]. Here we show that isotope disequilibrium in the $^3He/^4He$ ratio between helium trapped in vesicles and that dissolved in the glass phase of some young seamount basalts can be used to determine (U+Th)/He ages for the basalts. We use the $^3He/^4He$ in vesicles (extracted by crushing *in vacuo*) to correct the dissolved phase He (by fusion of the remaining powder) for the inherited component, and compute the radiogenic helium concentration. The method is applicable to rocks containing phases with different (U+Th)/He, and the results have implications for dating lavas in the age range of 10^3 to 10^6 years (thus filling a gap between the limits of the ^{14}C and K–Ar methods), and for reconstructing the geochemical history of young volcanic systems.

A suite of basaltic glasses from small seamounts near the East Pacific Rise at 10–14° N has been analysed. This seamount field erupts chemically diverse lavas ranging from tholeiite (with mid-ocean-ridge basalt (MORB) chemistry) to alkali basalt (from a source with time-integrated higher Rb/Sr, Nd/Sm and (U+Th)/He[7–9]). Here we report data for seamount 6, a small volcano (volume = 60 km^3; height = 1,300 m) located on 3 Myr-old seafloor (12°44′ N, 102°35′ W)[10]. This seamount consists of three coalesced volcanoes, which have erupted a broad range of lava types. In all but one case, the alkali-rich lavas show He isotope disequilibrium between vesicles and glass (Table 1; Fig. 1). The glass phase shows a clear radiogenic signature, with $^3He/^4He$ much less than the atmospheric ratio ($R_a = 1.4\times10^{-6}$). Because the alkalic rocks are both enriched in U and Th and have low He concentrations with respect to tholeiites[8,9], radiogenic ingrowth of ^4He is clearly detectable on the short timescale involved, that is 10^3 to 10^6 yr. Transitional basalts, presumably derived by mixing of tholeiitic and alkalic magmas[7,8], sometimes show He isotope disequilibrium. Only one of 22 tholeiites from this seamount field shows significant disequilibrium.

Following *in vacuo* crushing and analysis[11], the <100 μm fraction is transferred to a clean aluminium foil boat. The powders are then analysed for the remaining helium by melting *in vacuo* in a resistively heated Ta crucible, contained within a secondary vacuum envelope of a water-cooled furnace[12]. Furnace hot blanks are run before and after every sample. The average blank attributable to the Al boats is indetectable. The total processing blank for crushing and melting is the same, currently 4.3 ± 0.3 (one standard deviation) × 10^{-11} cm^3 STP He. Results for three samples of different ages have been replicated, and one sample (6B2) was also analysed by melting whole glass shards. Calculated ages for these cases are in agreement within analytical uncertainty (Table 1).

The minimum detectable age is dependent upon the U+Th content and the detection limit for He isotope disequilibrium.

† Present address: Department of Geological Sciences, Northwestern University, Evanston, Illinois 60201, USA.

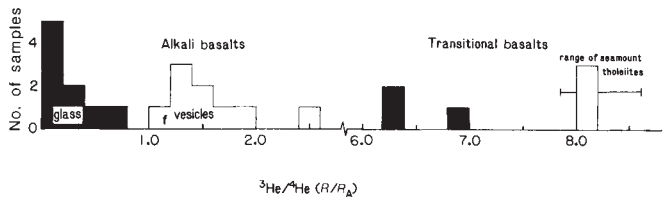

Fig. 1 Histogram of $^3He/^4He$ in samples showing isotopic disequilibrium between vesicles and glass at seamount 6. The range of $^3He/^4He$ in 22 other tholeiites and transitional basalts from young seamounts near the East Pacific Rise is shown for comparison.

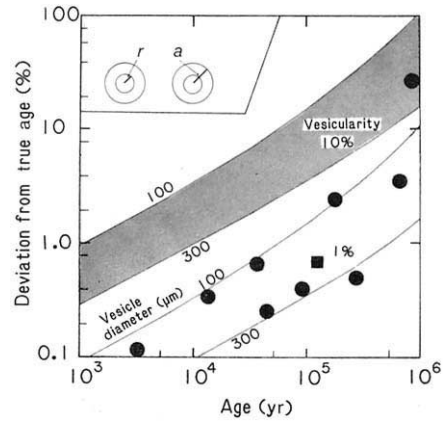

Fig. 2 Model for partial vesicle-glass equilibration by diffusion. The deviation (lowering) of the age T (in %) as a function of the true age is shown for vesicularities of 1% and 10% and a range of vesicle diameters from 100–300 μm. The diffusion coefficient, D, of He in basalt glass is 10^{-17} cm^2 s^{-1}, ref. 11. Vesicle geometry in this model is assumed to be the simplest case of homogeneously distributed spheres of uniform size; vesicle radius is r and diffusive radius $a = r+(DT)^{1/2}$. For low vesicularities (<10%) an individual vesicle domain is defined by a surrounding glass volume, $V = (p)(4\pi/3)r^3/(\text{ves})$, where ves is the volume fraction of vesicles and p is a geometric factor accounting for the vesicle packing fraction. A concentric shell in diffusive communication with a vesicle has a thickness approximated by $(DT)^{1/2}$, and volume $V_D = 4\pi/3\{(r+\sqrt{DT})^3 - r^3\}$. The fractional lowering (f) of the apparent age from the true age will be the fraction of $^4He^*$ missing from the glass which is lost to vesicles. For glass cubes with uniform U and Th distribution ($p = 8/(4\pi/3)$), $f = V_D/V = (\text{ves})(\pi/6)\{(r+\sqrt{DT})^3/r^3 - 1\}$. Circles are alkali basalts and the square is a transitional basalt from seamount 6. The diffusive effects are not appreciable in this model except in the case of the oldest sample.

The amount of radiogenic He produced in a time T (for $T < 10^7$ yr) is

$$^4He^* = 2.80\times10^{-8}\{[U](4.35+Th/U)\}T \ (\text{cm}^3\ \text{STP g}^{-1}) \quad (1)$$

where T is in Myr, Th/U is the atom ratio, and [U] is the uranium concentration in p.p.m. We use accepted decay constants[13] and assume secular equilibrium. The limiting factors in detecting ingrown ^4He are the reproducibility of the processing blank for analysis by mass spectrometry, and contamination from inherited He. For most of the present work the latter is the major limitation. The ^3He detection limit (~1.4 ± 3 × 10^{-17} cm^3 STP) may also become significant in distinguishing small age differences in very young samples. We estimate that the minimum detectable age is ~5,000 years for the sample types analysed here.

(U+Th)/He ages are calculated using several simplifying assumptions. The glass is assumed to be a closed system since

Table 1 Chemical analyses of seamount 6 basalts

					Crushed				Melted							
Sample	Rock type*	Mg no.	$(La/Sm)_N$	Vesicularity (vol. %)	Wt. (mg)	[He] 10^{-9} (cm^3 STP g^{-1})	$^3He/^4He$ (R/R_A)	±σ	Wt. (mg)	[He] 10^{-9} (cm^3 STP g^{-1})	$^3He/^4He$ (R/R_A)	±σ	$^4He^*$ 10^{-9} (cm^3 STP g^{-1})	U (p.p.m.)	Th (p.p.m.)	Age 10^3 yr
Rise D19-23†	AB	56.1	2.70	6.0	306.1	55.6	1.39	0.02	117.4	220	0.12	0.01	200	1.0	3.6	900±300
Rise D20-2	AB	52.5	1.90	1.0	190.4	9.9	1.39	0.05	93.9	19.9	0.33	0.05	15.2	0.79	2.8‖	88±10
Ceres D6-3	AB	51.9	2.72	0.5	123.1	3.5	1.86	0.28	96.8	15.0	0.14	0.07	13.9	1.52	5.02	43±3
Ceres D6B2	AB	54.3	2.84	1.5	175.7	10.4	1.58	0.07	70.5	15.7	0.42	0.10	11.6	1.47	5.25	36±4
replicate					369.0	9.4	1.51	0.15	105.0	13.5	0.36	0.10	10.3			32±4
whole glass shards									310.4	26.7	0.76	0.09				
Ceres D6-6‡	TH	65.1	0.28	ND	72.3	154	8.11	0.04	36.2	25.9	6.94	0.20	3.7	0.04	ND	500±500
ALV1388-1724	TR	65	1.13	ND	103.2	60.9	8.13	0.05	44.7	27.9	6.38	0.15	6.0	0.24	0.80	120±25
ALV1389-1613	AB	57.3	2.52	0.2	259.6	2.9	1.48	0.12	92.7	1.2	0.60	0.95	0.7	1.19	3.87	3±5
replicate					403.2	3.3	1.31	0.12	60.6	1.0	3.3	2.0	1			<4
ALV1389-1647	AB	55.0	2.90	ND	239.5	3.2	1.20	0.14	87.6	62.1	0.19	0.02	52.4	1.42	4.79	170±12
ALV1389-1810	AB	61.6	2.68	0.6	241.7	3.7	2.55	0.17	101.4	77.5	0.28	0.02	69.1	1.20	3.84	270±17
replicate					218.1	3.9	3.01	0.4	78.9	73.2	0.33	0.03	65.2			255±16
ALV1389-1854B	AB	54.7	ND	1.0	304.8	6.2	1.67	0.03	112.9	216	0.06	0.01	210	1.47	4.58	680±140
ALV1389-2115B	AB	56.0	2.9	1.3	295.9	6.3	1.32	0.07	118.4	4.5	0.05	0.18	4.3	1.57	5.18	13±3
ALV1391-2033	TR	64.6	1.16	0.4	210.2	57.3	8.17	0.03	89.7	17.7	6.24	0.10	4.2	0.16	0.78	100±33

ND, not determined. Crushed analyses are for 2-4 mm grain size; melted analyses are for the remaining <100 μm powder. U and Th determined by neutron activation analysis (ref. 8); typical uncertainties are 10% and less than 5%, respectively. Uncertainties in the computed ages include those associated with both U, Th and $^4He^*$ determinations. In most cases, analytical uncertainty for [U] contributes the largest error in the estimated age.

* AB, alkali basalt: TR, transitional basalt; TH, theoleiite.

† Micro-crystalline surface texture. All other samples show vitreous surfaces.

‡ ~10% of the glass in this sample is palagonitized. If the observed disequilibrium is partly due to retention of radiogenic He in palagonite, the computed age may be an upper limit.

§ Calculated from the relative constancy of K/U and Th/U in basalts; $K/U = 1.27 \times 10^4$ and Th/U = 3.5 (ref. 23); uncertainty in the ratios for these seamount basalts is ~30%.

‖ Calculated from measured [U] assuming Th/U = 3.5.

the time of eruption, with no isotope re-equilibration between vesicles and glass. The radiogenic He is

$$^4He^* = [He]_g\left\{\frac{R_v - R_g}{R_v - R_r}\right\} \quad (2)$$

where g and v refer to glass and vesicle phases and $R = (^3He/^4He)$. R_r, the radiogenic production ratio, depends upon sample composition and is between 10^{-8} and 10^{-7} for basalts[14-16]. ($^6Li(n, \alpha)^3H \rightarrow ^3He$, where the neutron production results from α-bombardment of Mg, Si and O target atoms, is by far the most important reaction producing ^3He *in situ* for seafloor basalts). Since $R_r \ll R_v$, approximating equation 2 as

$$^4He^* = [He]_g\{1 - (R_g/R_v)\}$$

does not presently introduce appreciable errors. Combining (1) and (2) gives

$$T = 3.58 \times 10^7\{[He]_g(1 - (R_g/R_v))/[U](4.35 + Th/U)\} \quad (3)$$

Some processes considered in the following discussion which could potentially affect inferred eruption ages include (i) atmospheric contamination; (ii) alteration of U and Th concentrations; (iii) implantation of α-particles from relatively U, Th-rich alteration surfaces and (iv) He loss from the glass.

Vesicularities of the samples range between 0.2 and 6 volume per cent (Table 1), with vesicle diameters between 0.1-0.5 mm. The ratio of ^3He trapped in vesicles to that dissolved in the glass is similar to the value determined for MORB at comparable vesicularities, where isotope disequilibrium has not been observed[11]. The fact that partitioning of inherited He (^3He) is similar for these different rock types suggests that no isotope fractionation occurred between gas and melt during eruption. Atmospheric contamination of the dissolved phase He is insignificant, as the $^3He/^4He$ ratio is much less than $1R_a$ and close to the theoretically predicted production ratio for basalts. In addition, the dissolved [He] in a basalt at equilibrium with air-saturated sea water is 2×10^{-9} cm^3 STP g^{-1} (for Henry's law constant $K = 3.7 \times 10^{-4}$ cm^3 STP g-atm^{-1}, refs 5, 11, 12), whereas measured concentrations in the alkali basalts range up to 2×10^{-7} cm^3 STP g^{-1}. At the present time we cannot exclude the possibility that the vesicles of these alkali basalts contain a fraction of an atmospheric (or sea-water) He component, but such contamination requires He migration along cracks because volume diffusion is too slow. We have found no evidence for the presence of significant cracks in either vesicle walls or the surrounding glass using the scanning electron microscope.

U and Th addition to glass could have varying effects on measured ages depending upon the degree of retention of the generated α-particles. Surficial U and Th may implant α-particles, but this process also causes some radiation damage, and most of the added He will likely be lost due to enhanced diffusion. Palagonite and manganese crusts are the most important U and Th-rich alteration phases[19,20]. We have avoided any significant contribution from alteration phases by careful cleaning and microscopic selection of very fresh samples that show vitreous surfaces on all sides.

Some possible mechanisms of He loss include migration along high diffusivity paths, α-ejection and volume diffusion of He, which might lead to loss from vesicles or glass, or to their partial isotope re-equilibration. Helium loss to high diffusivity paths is related to the population of micro-cracks, which ultimately depends upon the thermo-mechanical response of the glass to cooling and other changes. Significant (>10%) loss requires crack spacing to be ~10 times the diffusive distance for a given sample age, and of appropriate geometry that He loss is effective. For a diffusion coefficient (D_{He}) $\approx 10^{-17}$ cm^2 s^{-1} at sea-floor temperatures[11] and ages of 10^4 to 10^5 yr, crack scale lengths of 10 to 100 μm are required. We see no evidence for such cracks with the scanning electron microscope. Ultimately, weathering and devitrification are likely to be more important violations of glass remaining a closed system in (U+Th)/He dating, but careful sample selection avoids these problems.

The average α-stopping distance for a basalt glass is 20 μm. Only 25% of the ^4He generated within a surface layer of this thickness can be ejected from the sample[21]. Such a loss produces <1% uncertainty in the computed age for a sample from the outer 2 mm of a basalt pillow. Our samples are from pillow rims

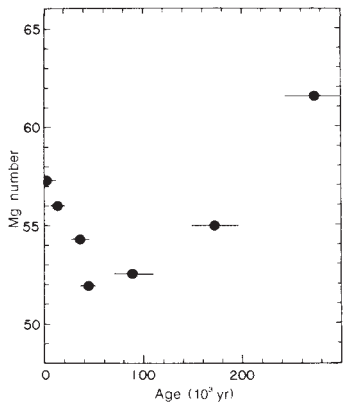

Fig. 3 Mg number ($\equiv 100 \times Mg/(Mg+Fe^{2+})$) against age for the youngest seamount 6 alkali basalts. ±2-sigma error estimates in the age are indicated.

typically 0.5–1.0 cm thick. The diffusion coefficient for He in basaltic glass is presently a point of debate[11,17], but firm upper limits for the extent of diffusive loss ($D_{He} \approx 10^{-15}$ cm^2 s^{-1} at sea-floor temperatures and 0.5 cm pillow rim thickness) are 4% and 11% in 10^4 yr and 10^5 yr, respectively. These losses, although significant, are comparable to our uncertainties.

We can estimate the extent of reequilibration between glass and vesicles using a simple diffusion model that assumes homogeneous distribution of spherical vesicles with uniform radius. Results of this model are shown in Fig. 2 along with the apparent age reduction that would occur for seamount 6 samples. The true age is increasingly underestimated as vesicularity increases and as vesicle size decreases. A typical deviation from the true age for our samples (10^5 yr, 1% vesicularity and 300 μm vesicle radius) is about 1%. Such a calculation is simplistic (for example, it neglects the size distribution of vesicles) but it demonstrates the relative magnitude of the reequilibration effect. Partial reequilibration between vesicles and glass also leads to lower vesicle $^3He/^4He$. Although this may be a significant effect (≥10%) on our estimate of the inherited $^3He/^4He$ for older samples, it has much less effect on the calculated age because the inherited component of the glass phase He is a smaller fraction of the measured [He]. In addition, if more than one vesicle size population is present, the larger vesicles (which are less affected by such reequilibration) will dominate the measured $^3He/^4He$ because of larger He contents. We conclude that although there are some inherent complications in the (U+Th)/He technique, the uncertainties introduced are comparable to, or less than, the analytical error for the studied samples.

At seamount 6, a pair of transitional basalts from the eastern satellite cone have similar ages (~10^5 yr). Another pair (the two Ceres 6 alkali basalts, dredged from a terrace between this eastern cone and the main vent[10]), also have similar ages (~40,000 yr). Collectively, the alkali basalts show a smooth trend in Mg number against age, with a minimum between 5×10^4 to 10^5 yr ago (Fig. 3). The approximate agreement between the age of the eastern cone and the age of the Mg number minimum suggests that a change in magmatic 'plumbing' occurred near this time. The event is marked by subsequent supply of less differentiated magma to the central volcanic complex. Although the spatial distribution of ages for the summit lavas (Rise and ALV1389 samples, see Table 1) is complex, they do not appear to violate principles of stratigraphic superposition. Additionally, the uniform ages obtained for the two distinct areas away from the main summit reinforce our contention that the ages are geologically meaningful, representing times of eruption, and thus provide a means to study volcanic evolution. The youth of the exposed lavas at seamount 6 has been confirmed by *Alvin* dive observations (for example, the lack of significant sediment cover) and is also consistent with magnetic gradiometer measurements[22]. All evidence points to volcanism occurring at seamount 6 at a significant distance off-axis of the East Pacific Rise.

We thank Teri Smith for access to unpublished seamount 6 data and for helpful discussions about its geology. We thank Tom Trull, Peter Meyer and Stan Hart for helpful and interesting discussions. We thank Dempsey Lott, whose careful engineering design, construction and modification of the mass spectrometer and sample processing system made the analyses possible. This work was supported by the NSF. D.G. thanks the Education Office of the MIT/WHOI Joint Program in Oceanography for financial support.

Received 21 July; accepted 11 December 1986.

1. Keevil, N. B. *Amer. J. Sci.* **241**, 680–693 (1943).
2. Hurley, P. M. *Geol. Soc. Amer. Bull.* **61**, 1–8 (1950).
3. Fanale, F. P. & Kulp, J. L. *Econ. Geol.* **57**, 735–746 (1962).
4. Damon, P. E. & Green, W. D. in *Proc. on the Symposium on Radioactive Dating* (Int. Atomic Energy Agency, Vienna 1963).
5. Damon, P. E. & Kulp, J. L. *Amer. Mineral.* **43**, 433–459 (1958).
6. Noble, C. S. & Naughton, J. J. *Science* **162**, 265–267 (1968).
7. Zindler, A. *et al. Earth planet. Sci. Lett.* **70**, 175–195 (1984).
8. Batiza, R. & Vanko, D. *J. geophys. Res.* **89**, 11235–11260 (1984).
9. Graham, D. W. *et al.* EOS **65**, 1079 (1984).
10. Batiza, R. & Vanko, D. *Mar. Geol.* **54**, 53–90 (1984).
11. Kurz, M. D. & Jenkins, W. J. *Earth planet. Sci. Lett.* **53**, 41–54 (1982).
12. Kurz, M. D., Jenkins, W. J. & Gurney, J. J. *Earth planet. Sci. Lett.* (in the press).
13. Steiger, R. H. & Jager, E. *Earth planet. Sci. Lett.* **36**, 359–362 (1977).
14. Morrison, P. & Pine, J. *Ann. N.Y. Acad. Sci.* **62**, 69–92 (1955).
15. Mamyrin, B. A. & Tolstikhin, L. N. *Helium Isotopes in Nature* (Elsevier, Amsterdam, 1984).
16. Andrews, J. N. *Chem. Geol.* **49**, 339–351 (1985).
17. Jambon, A., Weber, H. W. & Begemann, F. *Earth planet. Sci. Lett.* **73**, 255–267 (1985).
18. Marty, B. & Ozima, M. *Geochim. cosmochim. Acta* **50**, 1093–1097 (1986).
19. Newman, S. *et al. Earth planet. Sci. Lett.* **65**, 17–33 (1983).
20. MacDougall, J. D. *et al. Earth planet. Sci. Lett.* **42**, 27–34 (1979).
21. Bender, M. L. thesis, Columbia Univ. (1970).
22. McNutt, M. *J. geophys. Res.* **91**, 3686–3700 (1986).
23. Jochum, K. P. *et al. Nature* **306**, 431–436 (19833).

Electroreceptors in the platypus

J. E. Gregory, A. Iggo*, A. K. McIntyre & U. Proske

Department of Physiology, Monash University, Clayton, Victoria 3168, Australia

It has been known since the last century that the bill of the platypus contains densely packed arrays of specialized receptor organs and their afferent nerves. Until recently these were thought to be largely mechanoreceptive in function. However Scheich *et al.*[1] provide both behavioural and electrophysiological evidence that there are electroreceptors in the bill of the platypus. These authors were able to record evoked potentials from the somatosensory cortex of the brain in response to weak voltage pulses applied across the bill. Behavioural observations showed that a platypus could detect weak electric dipoles and it was suggested the animal was able to locate moving prey by the electrical activity associated with muscle contractions. From these observations, and in view of the fact that it was known that the bill contained gland receptors[2] which in several respects resembled the ampullary electroreceptors in freshwater fish, Scheich *et al.* concluded that the receptor array of the platypus bill included electroreceptors. In this report we present direct electrophysiological evidence for the existence of such receptors.

Discharges recorded in the infraorbital nerve which supplies the bill could be identified as coming from either mechanoreceptors or electroreceptors. Electroreceptors could be readily distinguished from mechanoreceptors as the electroreceptors showed

* Permanent address: Department of Preclinical Veterinary Sciences, University of Edinburgh, Summerhill, Edinburgh EH9 1QH, UK.